INSTITUTE OF PHYSICS PUBLISHING JOURNAL OF PHYSICS B: ATOMIC, MOLECULAR AND OPTICAL PHYSICS

J. Phys. B: At. Mol. Opt. Phys. **38** (2005) 3795–3804 doi:10.1088/0953-4075/38/21/002

A theoretical study on elastic electron–CH_x (x = 1, 2, 3, 4) collisions in the low-energy range

M-T Lee[1], L E Machado[2], L M Brescansin[3] and I Iga[1]

[1] Departamento de Química, UFSCar, 13565-905 São Carlos, SP, Brazil
[2] Departamento de Física, UFSCar, 13565-905 São Carlos, SP, Brazil
[3] Instituto de Física 'Gleb Wataghin', UNICAMP 13083-970 Campinas, SP, Brazil

Received 13 June 2005, in final form 24 August 2005
Published 10 October 2005
Online at stacks.iop.org/JPhysB/38/3795

Abstract

In this work, a theoretical study on elastic electron–CH_x (x = 1, 2, 3, 4) collisions in the low-energy range is presented. More specifically, calculated elastic differential, integral and momentum transfer cross sections are reported in the (0.1–20) eV energy range. An optical potential formed by static, exchange and correlation–polarization contributions is used to represent the electron–target interaction, while the iterative Schwinger variational method is used to solve the scattering equations. Comparison of the calculated results for electron scattering by these targets shows an interesting trend.

1. Introduction

Interest on electron collisions with highly reactive radicals such as CH_x, CF_x (x = 1, 2, 3), etc has grown recently, in view of their important applications in several areas [1, 2]. For instance, plasma environments are composed by many species such as electrons, molecules in their ground and excited states, neutral radicals, ionic fragments, etc. The knowledge of cross sections for electron interaction with all the constituents would be important for plasma modelling. Specifically, the CH_x radicals (x = 1, 2, 3) are important fragments produced from dissociation of CH_4 either by collisional interaction and/or photodissociation. Methane is an important constituent of the terrestrial and other planetary (Jupiter, Saturn, Uranus, etc) atmospheres. It is also frequently used as a constituent of feedgas in technological processing plasmas for deposition purposes (diamond films, diamond-like carbon films, amorphous carbon films) [3–8]. Therefore, various cross sections for e^-–CH_x collisions are expected to be important for the understanding and modelling of the chemistry in both planetary atmospheres and discharge plasmas. Unfortunately, the experimental determination of such cross sections is difficult. Only a limited set of electron-impact ionization cross sections of a few molecular radicals was reported in the literature [9–12]. Therefore, theoretical calculations are presently important to provide electron-radical scattering cross sections. Recently, e^--radical collisions have been a subject of increasing number of theoretical investigations.

Joshipura and Vinodkumar [13] and Joshipura *et al* [14] have reported grand total cross sections (TCS's) and total absorption cross sections (TACS's) for electron scattering by several CH_x, NH_x and OH radicals in the intermediate and high energy range. More recently, Baluja *et al* [15] reported an *R*-matrix calculation of elastic and excitation cross sections for low-energy electron collisions with ClO. Also, theoretical studies for electron scattering by several radicals [16–18] have been reported by our group in recent past.

On the theoretical side, studies on low-energy electron scattering by CH_x ($x = 1, 2, 3$) are also scarce. To our knowledge, the only such study in the literature is the *R*-matrix calculation for e^-–CH collisions, performed by Baluja and Msezane [19]. Other calculations for e^-–CH_x collisions [13, 14] have been restricted to TCS's and TACS's in the (20–3000) eV range. A complex optical potential and additivity rules were used in those calculations. It is well known that the kinetic energy of most electrons present in plasma environments lies below 20 eV. Thus, low-energy electron scattering cross sections are interesting for such applications. Also, from the theoretical point of view, the differential cross sections (DCS's) are much more sensitive than TCS's and TACS's to the interaction potentials, therefore providing a better test for new theoretical developments.

Taking into account the above considerations and aiming at fulfilling the lack of data for such collisions, we present a theoretical study on electron scattering by CH_x ($x = 1, 2, 3, 4$) targets. Specifically, calculated elastic DCS's, integral (ICS's) and momentum-transfer (MTCS's) cross sections in the (0.1–20) eV energy range are reported. The present study made use of an optical potential to represent the interaction dynamics, while the iterative Schwinger variational method (ISVM) [20, 21] is used to solve the scattering equations. This procedure has already been successfully applied to studies of electron scattering by a number of molecules [22, 23], and thus it is expected to be successful also for e^--radical collisions.

The organization of this paper is as follows: in section 2, we describe briefly the theory used and also give some details of the calculation. In section 3, we present our calculated results and compare them with some selected experimental data for e^-–CH_4 collisions. A brief conclusion is also summarized in this section.

2. Theory and calculation

In this section we will briefly discuss the method used; details of the ISVM can be found elsewhere [18, 20]. Within the adiabatic-nuclei-rotation framework, the DCS's for the excitation for an asymmetric-top rotor from an initial rotational level $J\tau$ to a final level $J'\tau'$ are given by

$$\frac{\mathrm{d}\sigma}{\mathrm{d}\Omega}(J\tau \longrightarrow J'\tau') = \frac{1}{(2J+1)}\frac{k}{k_0}\sum_{M=-J}^{J}\sum_{M'=-J'}^{J'}|f_{J\tau M\longrightarrow J'\tau'M'}|^2, \tag{1}$$

where $f_{J\tau M\longrightarrow J'\tau'M'}$ is the rotational excitation scattering amplitude related to the rotational eigenfunctions of the target by

$$f_{J\tau M\longrightarrow J'\tau'M'} = \langle\Psi_{J'\tau'M'}(\Omega)|f^{LF}|\Psi_{J\tau M}(\Omega)\rangle, \tag{2}$$

k_0 and k are the magnitudes of the initial and final linear momenta of the scattering electrons, respectively, and $\Omega \equiv (\alpha, \beta, \gamma)$ are the Euler angles defining the direction of the target principal axes in the laboratory frame (LF). The eigenfunctions $\Psi_{J\tau M}(\Omega)$ appearing in equation (2) are written as linear combinations of symmetric-top eigenfunctions [24]:

$$\Psi_{J\tau M}(\Omega) = \sum_{K=-J}^{J} a_{KM}^{J\tau}\Phi_{JKM}(\Omega), \tag{3}$$

where

$$\Phi_{JKM}(\Omega) = \left(\frac{2J+1}{8\pi^2}\right) D^{J^*}_{KM}(\Omega), \tag{4}$$

D^J_{KM} being the well-known Wigner rotation matrices [25]. Also, f^{LF} appearing in equation (2) is the electronic part of the LF scattering amplitude which can be related to the corresponding body-frame (BF) T matrix by an usual frame transformation [25]. The latter can be conveniently partial-wave expanded as

$$T = \frac{1}{k} \sum_{p\mu lhl'h'} \mathrm{i}^{l-l'} T^{p\mu}_{k,lh;l'h'} X^{p\mu}_{lh}(\hat{k}) X^{p\mu^*}_{l'h'}(\hat{k}_0) \tag{5}$$

where $\hat{k}_0$ and $\hat{k}$ are the linear momentum directions of the incident and scattered electrons in BF, respectively, and $X^{p\mu}_{lh}(\hat{k})$ are the symmetry-adapted functions [26] which are expanded in terms of the usual spherical harmonics as follows:

$$X^{p\mu}_{lh}(\hat{r}) = \sum_m b^{p\mu}_{lhm} Y_{lm}(\hat{r}). \tag{6}$$

Here p is an irreducible representation (IR) of the molecular point group, μ is a component of this representation and h distinguishes between different bases of the same IR corresponding to the same value of l. The coefficients $b^{p\mu}_{lhm}$ satisfy important orthogonality relations and are tabulated for C_{2v} and O_h point groups [26].

The rotationally unresolved DCS's for elastic e^--molecule scattering are calculated through a summation of all rotationally resolved DCS's

$$\frac{\mathrm{d}\sigma}{\mathrm{d}\Omega} = \sum_{J'\tau'} \frac{\mathrm{d}\sigma}{\mathrm{d}\Omega}(J\tau \longrightarrow J'\tau'). \tag{7}$$

In our calculations, the e^--radical scattering dynamics is represented by an optical potential formed by static (V_{st}), exchange (V_{ex}) and correlation–polarization (V_{cp}) contributions. V_{st} and V_{ex} are obtained exactly from a Hartree–Fock (HF) self-consistent-field (SCF) target wavefunction. A parameter-free model potential introduced by Padial and Norcross [27] is used to account for the correlation–polarization contributions. In this model, a short-range correlation potential between the scattering and the target electrons is defined in an inner region and a long-range polarization potential in an outer region. The first crossing of the correlation and polarization potential curves defines the inner and the outer regions. The correlation potential is calculated by a free-electron-gas model, derived from the target electronic density according to equation (9) of [27]. In addition, the asymptotic form of the polarization potential is used for the long-range electron–target interaction. Since there are no reported experimental dipole polarizabilities for CH_x ($x = 1, 2, 3$), they were calculated by us using an HF–SCF procedure and used to generate the asymptotic form of V_{cp}. No cutoff or other adjusted parameters are needed for the calculation of the correlation–polarization contribution. Alternative model polarization potentials could also be used in our calculation. As a matter of fact, test runs were carried out using the sharp cutoff potential of Jain [28] for electron scattering by CH_3 and CH_4. The results of such tests come in support of our choice of V_{cp}.

The ground-state electronic configurations for CH, CH_2, CH_3 and CH_4 are: $1\sigma^2 2\sigma^2 3\sigma^2 1\pi^1, X^2\Pi$; $1a_1^2 2a_1^2 1b_2^2 3a_1^1 1b_1^1, X^3B_1$; $1a_1'^2 2a_1'^2 1e'^4 1a_2''^1, X^2A_2''$; and $1a_1^2 2a_1^2 t_2^6$, X^1A_1, respectively. Since CH_x ($x = 1, 2, 3$) are open-shell radicals, different total spin-specific states of the (e^-+CH_x) system are considered in the present study. Explicitly, singlet and triplet couplings are considered for electron scattering by the CH and CH_3 radicals, whereas doublet

Table 1. Cartesian Gaussian functions used in the SCF calculations[a].

Atom	s		p		d	
	Exp.	Coeff.	Exp.	Coeff.	Exp.	Coeff.
	4232.61	0.006 228	18.1557	0.039 196		
	634.882	0.047 676	3.986 40	0.244 144		
	146.097	0.231 439	1.142 90	0.816 775		
	42.4974	0.789 108				
C	14.1892	0.791 751				
	1.966 60	0.321 870				
	5.147 70	1.000 000	0.359 40	1.000 000	0.756	1.000 000
	0.496 20	1.000 000	0.165 40	1.000 000	0.150	1.000 000
	0.153 30	1.000 000	0.082 50	1.000 000	0.0375	1.000 000
	0.047 30	1.000 000	0.036 50	1.000 000		
	0.012 50	1.000 000	0.012 50	1.000 000		
	0.004 50	1.000 000	0.003 50	1.000 000		
	19.2384	0.032 828	26.7900	0.018 254		
	2.898 72	0.231 204	5.956 00	0.116 461		
H	0.653 472	0.817 226	1.707 00	0.390 178		
	0.163 064	1.000 000	0.531 400	0.637 102		
	0.101 309	1.000 000	0.300 00	1.000 000		
			0.120 00	1.000 000		
			0.040 00	1.000 000		

[a] Cartesian Gaussian basis functions are defined as $\phi^{\alpha,\ell,m,n,\mathbf{A}}(\mathbf{r}) = N(x-\mathbf{A}_x)^{\ell}(y-\mathbf{A}_y)^{m}(z-\mathbf{A}_z)^{n}\exp(-\alpha|\mathbf{r}-\mathbf{A}|^2)$, with N a normalization constant.

Table 2. Calculated properties of the CH_x ($x = 1, 2, 3, 4$) molecules.

	CH	CH_2	CH_3	CH_4
Energy (Hartree)	−38.1617	−38.9294	−39.5693	−40.1987
Dipole moment(D)	1.470	0.583	0.0	0.0
α_{00} (au)	13.2817	13.5600	15.2229	17.5[a]
α_{20} (au)	2.2434	1.1986	0.089 36	0.0
α_{22} (au)	0.0	0.053 49	0.0	0.0

[a] Experimental value of [29].

and quartet couplings are taken into account for e^-–CH_2 collisions. Therefore, the statistical average of the elastic scattering DCS's is written as

$$\frac{d\sigma}{d\Omega} = \frac{1}{a+b}\left[a\left(\frac{d\sigma}{d\Omega}\right)^{S_1} + b\left(\frac{d\sigma}{d\Omega}\right)^{S_2}\right] \tag{8}$$

where $(d\sigma/d\Omega)^{S_i}$ $(i = 1, 2)$ are the multiplet-specific DCS's averaged over molecular orientations for the total (e^-+CH_x) spin S_i, and a (b) is the statistic weight of the particular total spin state S_1 (S_2). Explicitly, for CH and CH_3, $S_1 = 0$ (singlet), $S_2 = 1$ (triplet), $a = 1$, and $b = 3$; for CH_2, $S_1 = 1/2$ (doublet), $S_2 = 3/2$ (quartet), $a = 1$, and $b = 2$.

In this study, the target wavefunctions are calculated using an HF-SCF procedure. The basis set used for this calculation is shown in table 1. The calculated SCF energies and permanent dipole moments at the experimental equilibrium geometry of the ground-state CH_x targets [30] are shown in table 2, where we also present the calculated dipole polarizabilities. Particularly, our calculated permanent dipole moment for CH (1.47 D) is in good agreement with the value of 1.46 D quoted by Itikawa [31].

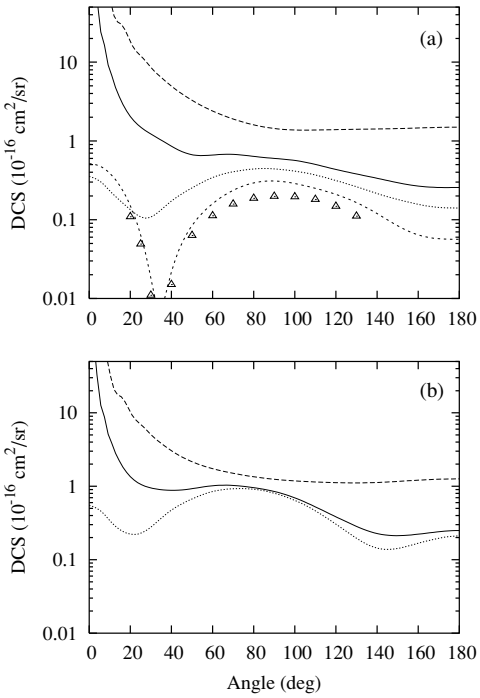

Figure 1. DCS's for elastic e^-–CH_x ($x = 1, 2, 3, 4$) scatterings at (a) 1 eV and (b) 2 eV. Full curve, calculated results for e^-–CH_2; dashed line, calculated results for e^-–CH; dotted line, calculated results for e^-–CH_3; short-dashed line, calculated DCS's for e^-–CH_4; open triangles, experimental data of Sohn *et al* [33] for e^-–CH_4.

In our calculations, the partial-wave expansion of the continuum wavefunctions as well as of the T-matrix elements are limited to $l_{\max} = 16$ and $m_{\max} = 16$. Since CH and CH_2 are polar radicals, these partial-wave expansions converge slowly due to the long-range dipole interaction potential. Therefore, a Born-closure formula is used to account for the contribution of higher partial-wave components to the scattering amplitudes. Accordingly, equation (5) is rewritten as

$$T = T^B + \frac{1}{k}\sum_{p\mu lhl'h'}^{LL'} i^{l-l'}\left(T^{p\mu^{\mathrm{ISVM}}}_{k,lh;l'h'} - T^{p\mu^B}_{k,lh;l'h'}\right) X^{p\mu}_{lh}(\hat{k}) X^{p\mu^*}_{l'h'}(\hat{k}_0) \tag{9}$$

where T^B is the complete point-dipole first-Born-approximation (FBA) T-matrix, $T^{p\mu^{\mathrm{ISVM}}}_{k,lh;l'h'}$ are the partial-wave T-matrix elements calculated via ISVM and $T^{p\mu^B}_{k,lh;l'h'}$ are the corresponding partial-wave point-dipole FBA T-matrix elements, given by

$$T^{p\mu^B}_{k,lh;l'h'} = -\frac{D}{L}\left[\frac{(L+h)(L-h)}{(2L+1)(2L-1)}\right]^{\frac{1}{2}}, \tag{10}$$

where D is the target electric dipole moment and $L = l'$ when $l' = l + 1$ and $L = l$ when $l' = l - 1$.

3. Results and discussion

In figures 1–3 we show our calculated DCS's (rotationally summed) for elastic e^-–CH_x ($x = 1, 2, 3, 4$) scattering in the (1–20) eV energy range. Unfortunately, there are no

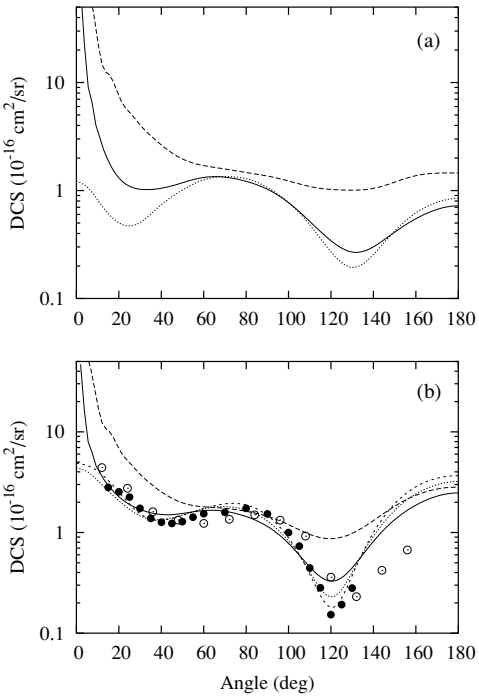

Figure 2. Same as in figure 1, but for (a) 3 eV and (b) 5 eV. Full circles, experimental DCS's of Boesten and Tanaka [34] for e^-–CH_4; open circles, experimental DCS's of Shyn and Cravens, [35] for e^-–CH_4.

experimental results for the studied radicals available in the literature; therefore; only the experimental results for the e^-–CH_4 collisions [33–35] are shown for comparison. At low incident energies, there are significant differences, both qualitatively and quantitatively (see figures 1 and 2), among the calculated DCS's for electron scattering by the four targets. It is well known that at very low energies, where the incident electron has less penetration power into the target electronic cloud, the long-range interactions of both permanent and/or induced dipolar nature are dominant in the collisional dynamics. Moreover, for polar targets such as CH (1.47 D) and CH_2 (0.583 D), the permanent dipole interaction between the target and the scattering electron is more important than the polarization nature of potential. These behaviours are clearly observed in the calculated DCS's. At 1 and 2 eV, the calculated DCS's for electron scattering from the strongly polar CH radical lie well above those from other three targets. Moreover, the DCS's for e^-–CH and e^-–CH_2 are sharply enhanced at the forward direction, indicating the strong influence of the dipolar interaction. However, the penetration power of the incident electron increases with increasing energy. Therefore, the interaction between the incident electron and the target electrons becomes dominant in the collisional dynamics at incident energies of 10 eV and above. For such energies, one observes a remarkable similarity among the DCS's for electron scattering from the four targets, as can be seen in figure 3. This similarity clearly indicates that the electron scattering interaction dynamics in the (10–20) eV energy range for these targets is dominated by the much heavier central carbon atom.

Tables 3 and 4 show our ICS's and MTCS's, respectively, calculated for elastic e^-–CH_x ($x = 1, 2, 3, 4$) collisions in the (0.1–20) eV range. These data are also shown

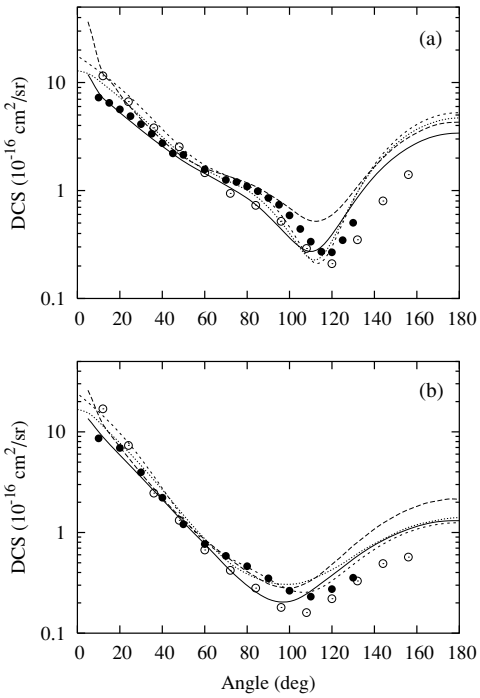

Figure 3. Same in as figure 2, but for (a) 10 eV and (b) 20 eV.

Table 3. ICS's (in 10^{-16} cm^2) for e^-–CH_x ($x = 1, 2, 3, 4$) scattering.

Energy (eV)	CH	CH_2	CH_3	CH_4
0.1			2.567	3.266
0.3			1.909	0.923
0.5		17.82	2.401	1.030
1	57.83	12.29	3.883	2.360
2	35.76	11.13	6.739	
5	28.18	16.18	16.15	17.48
10	25.60	18.74	22.81	25.84
15	20.80	16.23	19.76	22.54
20	17.09	13.74	16.79	18.33

in figures 4(a) and (b), along with the experimental results for e^-–CH_4 scattering [33–35]. On qualitative aspects, minimum features are located at about 0.3 eV in the calculated ICS's for CH_3 and CH_4. These features are identified as Ramsauer–Townsend minima. In addition, a minimum is also clearly seen in the calculated ICS's for CH_2 at about 1.2 eV. In contrast, this minimum is not of Ramsauer–Townsend nature. In order to understand its physical origin, in figures 5(a) and (b) we present the energy dependence of the s-wave ($l = 0$) eigenphase δ_0 for both e^-–CH_2 (doublet and quartet couplings) and e^-–CH_3 (singlet and triplet couplings) scatterings, respectively. It is clearly seen that δ_0 for the triplet coupling of CH_3 and the quartet coupling of CH_2 are null at about 0.3 eV, indicating the occurrence of a Ramsauer–Townsend minimum. On the other hand, no such minima were identified in the singlet coupling of CH_3 and the doublet coupling of CH_2 scatterings. It is interesting to note that despite CH_2 is

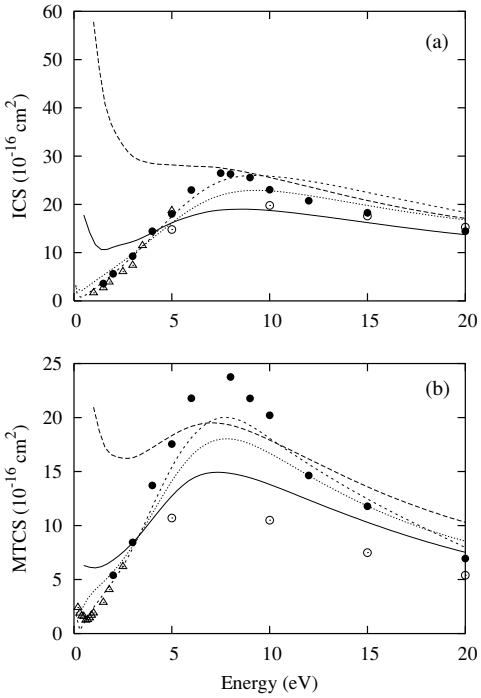

Figure 4. (a) ICS's and (b) MTCS's for elastic electron scattering by CH_x ($x = 1, 2, 3, 4$) in the (1–20) eV range. The symbols are the same as in figures 1 and 2.

Table 4. MTCS's (in 10^{-16} cm^2) for e^-–CH_x ($x = 1, 2, 3, 4$) scattering.

Energy (eV)	CH	CH_2	CH_3	CH_4
0.1			1.884	1.790
0.3			1.886	0.320
0.5		6.310	2.642	0.890
1	20.96	6.077	3.901	2.410
2	16.47	6.810	5.716	
5	18.32	12.73	14.11	15.40
10	17.91	13.81	16.69	18.08
15	13.59	10.30	11.81	12.37
20	10.30	7.525	8.564	7.975

moderately polar and CH_3 and CH_4 are nonpolar, the physical origin leading to the occurrence of Ramsauer–Townsend minimum in these targets would be the same. The interaction between the scattering electron and the carbon atom is probably responsible for this occurrence because no centrifugal barrier is present for s-wave scattering and even electrons with kinetic energies as low as 0.3 eV can penetrate into the target and so interact with nuclei and inner-shell electrons. On the other hand, the minimum at about 1.2 eV seen in the calculated ICS's of CH_2 is due to the combination of two effects, the decrease of the ICS's towards lower energies (that would be responsible for the existence of a Ramsauer–Townsend minimum at 0.3 eV if no dipole interaction were present), and the pronounced enhancement of ICS's at low incident energies due to the dominant dipole interaction for polar targets. Quantitatively, the calculated ICS's and MTCS's for the e^-–CH scattering lie significantly above those of the other three targets

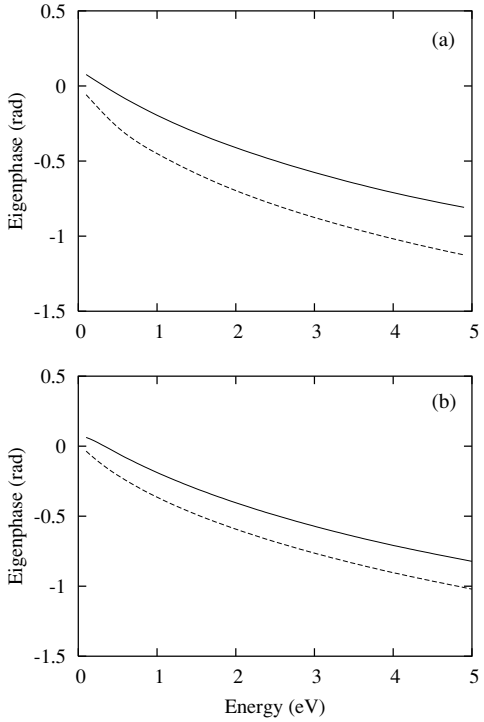

Figure 5. (a) Spin-specific s-wave eigenphase for e^-–CH_2 scattering. Solid line, results for the quartet coupling; dashed line, for the doublet coupling; and (b) spin-specific s-wave eigenphase for e^-–CH_3 scattering. Solid line, results for the triplet coupling; dashed line, for the singlet coupling.

at the lower end of incident energies, due to the strong dipole moment of CH. Nevertheless, ICS's and MTCS's for the four targets become more similar with increasing incident energies, indicating that the electron–carbon atom interaction becomes more important when electron penetrates more into the targets.

In summary, we report a theoretical study on the elastic electron scattering by CH_x ($x = 1, 2, 3, 4$) in the low and intermediate energy range. We expect that the present study can stimulate further theoretical investigations. Also, in view of the scarcity of both theoretical and experimental cross sections for electron scattering by these important radicals, it is hoped that the results reported in the present study can be useful for applications in plasma modelling and atmospheric studies.

Acknowledgments

This work was partially supported by the Brazilian agencies FAPESP and CNPq.

References

[1] Janev R K 1993 *Atomic and Plasma-Material Interaction Processes in Controlled Thermonuclear Fusion* ed R K Janev and H W Drawin (Amsterdam: Elsevier) p 27
[2] Wang W and Sze N D 1980 *Nature* **286** 589
[3] Tang Y X and Aslam D M 2005 *J. Vacuum Sci. Technol.* B **23** 1088
[4] Peng G, Jun X, Deng X L, Wang D H and Chuang D 2005 *Acta Phys. Sin.* **54** 3241

[5] Choi B G, Kim J K, Yang W J and Shim K B 2005 *J. Ceram. Process. Res.* **6** 101
[6] Ikuno T, Honda S, Kamada K, Oura K and Katayama M 2005 *J. Appl. Phys.* **97** 104329
[7] Tzeng Y and Liu Y K 2005 *Diam. Relat. Mater.* **14** 261
[8] Iizuka S, Nishimura G, Ikeda R and Yamaguchi H 2005 *Diam. Relat. Mater.* **14** 279
[9] Tarnovsky V, Deutsch H and Becker K 1996 *J. Chem. Phys.* **109** 932
[10] Tarnovsky V, Deutsch H and Becker K 1997 *Int. J. Mass. Spectrom. Ion Process.* **167** 69
[11] Tarnovsky V, Levin A, Deutsch H and Becker K 1996 *J. Phys. B: At. Mol. Opt. Phys.* **29** 139
[12] Tian C and Vidal C R 1998 *J. Phys. B: At. Mol. Opt. Phys.* **31** 895
[13] Joshipura K N and Vinodkumar M 1997 *Phys. Lett.* A **224** 361
[14] Joshipura K N, Vinodkumar M and Patel U M 2001 *J. Phys. B: At. Mol. Opt. Phys.* **34** 509
[15] Baluja K L, Mason N J, Morgan L A and Tennyson J 2000 *J. Phys. B: At. Mol. Opt. Phys.* **33** L677
[16] Lee M T, Lima M F, Sobrinho A M C and Iga I 2002 *J. Phys. B: At. Mol. Opt. Phys.* **35** 2437
[17] Lee M T, Lima M F, Sobrinho A M C and Iga I 2002 *Phys. Rev.* A **66** 062703
[18] Sobrinho A M C, Lozano N B H and Lee M T 2004 *Phys. Rev.* A **70** 032717
[19] Baluja K L and Msezane A Z 2001 *J. Phys. B: At. Mol. Opt. Phys.* **34** 3157
[20] Lucchese R R, Raseev G and McKoy V 1982 *Phys. Rev.* A **25** 2572
[21] Lee M T, Michelin S E, Machado L E and Brescansin L M 1993 *J. Phys. B: At. Mol. Opt. Phys.* **26** L203
[22] Iga I and Lee M T 1999 *J. Phys. B: At. Mol. Opt. Phys.* **32** 453
[23] Iga I, Lee M T, Homem M G P, Machado L E and Brescansin L M 2000 *Phys. Rev.* A **61** 022708
[24] Jain A and Thompson D G 1983 *Comput. Phys. Commun.* **30** 301
[25] Rose M E 1957 *Elementary Theory of Angular Momentum* (New York: Wiley)
[26] Burke P G, Chandra N and Gianturco F A 1972 *J. Phys. B: At. Mol. Phys.* **5** 2212
[27] Padial N T and Norcross D W 1984 *Phys. Rev.* A **29** 1742
[28] Jain A 1986 *Phys. Rev.* A **34** 3707
[29] Börnstein Landolt 1951 *Zahlenwerte und Funktionen* vol 1 part 3 (Berlin: Springer) p 511
[30] Lide D V (ed) 1993 *Handbook of Chemistry and Physics* 73rd edn (Boca Raton, FL: CRC Press)
[31] Itikawa Y 1978 *Phys. Rep.* **46** 117
[32] Machado L E, Lee M T and Brescansin L M 1998 *Braz. J. Phys.* **28** 111
[33] Sohn W, Kochem K H, Scheuerlein K M, Lung K and Ehrhardt H 1986 *J. Phys. B: At. Mol. Phys.* **19** 3625
[34] Boesten L and Tanaka H 1991 *J. Phys. B: At. Mol. Opt. Phys.* **24** 821
[35] Shyn T W and Cravens T E 1990 *J. Phys. B: At. Mol. Opt. Phys.* **23** 293